Determination method of Markstein number based on wavenumber measurement of cellular flames at the onset of parametric instability of downward propagating flames

Jerric R. Delfin[a,b], Feng Guo[a], Nozomu Hashimoto[a], Osamu Fujita[a*]

[a]*Division of Mechanical and Space Engineering, Hokkaido University, Kita 13 Nishi 8 Kita-ku, Sapporo, Hokkaido 060-8628, Japan*
[b]*Department of Mechanical Engineering, College of Engineering and Agro-Industrial Technology, University of the Philippines Los Baños, Los Baños, Laguna 4031, Philippines*

Abstract

This work proposes a new method to estimate the Markstein number by investigating the thermoacoustic parametric instability of laminar premixed flames propagating downwards in an open-closed tube. Methane-air flames were propagated in a combustion tube to capture the flame evolution in transition to parametric instability. By synchronized high-speed imaging filming both lateral and longitudinal views of flame propagation, cellular flame wavenumbers are measured from the clear transition of flat flames to cellular flames visualized in the present approach. The Markstein number is indirectly determined from wavenumber measurements at the onset of parametric instability by employing a laminar flame model under acoustic excitation treating the Markstein number as a free parameter. Acoustic velocity fluctuation amplitudes obtained from pressure fluctuation measurements were determined to further evaluate the validity of wavenumber-derived Markstein numbers. Markstein numbers obtained in the present work are compared with Markstein numbers relative to fresh gases in the literature from indirect and computational methods.

Keywords: Thermoacoustic parametric instability; Combustion tube; Cellular premixed flames; Wavenumber; Markstein number

---

*Corresponding author.

1) Novelty and Significance Statement

This work introduces a novel method to determine the Markstein number based on the flame structure of thermoacoustically unstable laminar premixed flame. The indirect measurement of Markstein number based on wavenumber measurements at the onset of parametric instability of downward propagating flames has not been previously explored. The wavenumber-derived Markstein number in this work is validated by acoustic velocity measurements derived from pressure fluctuation data. The clear transition of flat flames to cellular flames is also visualized in the present work for the first time. This method to indirectly determine the Markstein number offers simplicity and efficiency since each experiment effectively yields a set of wavenumber measurements to give a statistical estimate of the Markstein number, whereas other indirect methods existing in the literature require several separate experiments to obtain a representative set of data.

2) Author Contributions

All authors contributed to the conceptualization and design of the study.

- J.R.D.: experiments, formal analysis, and writing – original draft.
- F.G.: analysis, validation, and writing – review and editing.
- N.H.: analysis, validation, writing – review and editing.
- O.F.: analysis, writing – review and editing, supervision.

All authors discussed the results and approved the final manuscript.

3) Authors' Preference and Justification for Mode of Presentation at the Symposium

The authors prefer the **OPP** presentation at the Symposium, for the following reasons:

- There are several methods to indirectly measure the Markstein number. Since the current work presents a retroactive approach, the procedure needs to be discussed thoroughly and results can be better understood if explained orally.
- The parametric instability of laminar premixed flames is an interesting phenomenon that can be better appreciated if presented orally and supplemented by videos.
- This work shows the difference in Markstein numbers relative to fresh gases (which are limited but dispersed in literature) obtained from different methods.

1. Introduction

Thermoacoustic instabilities arise due to the complex dynamic interaction between combustor acoustics and unsteady heat release which constitute a challenging problem in the field of combustion science and nonlinear dynamics. These instabilities may arise due to intrinsic factors such as gas expansion, differences in heat and mass diffusion rates, gravity, and external causes such as flame front interaction with self-generated acoustics. Pressure perturbations can be amplified when the heat release of reactive fronts and acoustic pressure are in phase according to the well-cited Rayleigh criterion [1]. Instabilities can grow or decay depending on the competition between the acoustic energy from flame-acoustics interaction and damping mechanisms such as heat and wall loss.

Flame-acoustics interaction can be studied in confined chambers as demonstrated by Searby [2] with downward propagating flames in open-closed tubes. Flames ignited at the top and freely propagating downwards are inherently prone to thermoacoustic instabilities. Generally, two types of instabilities are observed during flame propagation: primary and secondary instability [2]. Primary instability is observed at moderate laminar burning velocities (S_L) when the curved flame due to Darrieus-Landau (D-L) instability is stabilized by acoustic waves forming a planar flame. The amplitude of the vibrating planar flame increases with time and saturates at a constant amplitude. At sufficiently fast S_L and higher acoustic oscillations, the flat flame can transition to secondary instability. In this regime, the flat flames transform into cellular structures of certain wavenumber that grow in amplitude and oscillate twice the period of the acoustic standing of the tube, abruptly changing the surface structure of the combustion front leading to turbulent flame propagation. At even higher S_L, stable flat flames may disappear due to "complete" instability when the initially curved flame successively transitions to secondary instability [3]. Secondary instability is caused by parametric instability due to the acoustic acceleration of the flame front whose mechanism is similar to Faraday instability as concluded by Markstein [4]. Pressure oscillation amplitudes and growth rates during secondary instability are much higher compared to primary instability.

The simplicity of Searby's experiments [2] allows the premixed flame to propagate freely such that vorticity, inhomogeneity and equivalence ratio fluctuations are eliminated or otherwise minimized. The flame can be treated as laminar, such that flame instability can be modeled and theoretically studied through large activation energy asymptotics treating the flame front as a discontinuity [5,6]. Searby and Rochwerger [6] managed to calculate stability diagrams of acoustically excited laminar flames predicting the critical wavenumbers and acoustic velocity amplitudes on the onset, disappearance and coexistence of D-L and parametric instabilities, and their growth rates. Later, Bychkov [7] simplified the formulation and derived explicit functions for the marginal limits of stability but posed limiting conditions. Aldredge [8] modified the formulation to accommodate the influence of viscosity on thermoacoustic instability for flames propagating in annular chambers with closely separated walls. Recently, stability diagrams obtained from the original formulation [6] have been used to interpret the complete disappearance of flat flames of hydrocarbon flames [3], acoustic-parametric instability of lean hydrogen-air mixtures [9,10] and of $CH_4/O_2/Xe$ mixtures [11]. Since the seminal work of Searby [2], there have been several experimental works conducted to gain a better understanding of flame-acoustics phenomena of downward propagating flames in tubes [3,11-16] and similar experimental configurations [8,10,17-20].

The influence of flame stretch and curvature on the response of the acoustically forced flame, characterized by the Markstein number (*Ma*), has been accounted for and is an important parameter in the formulation of stability diagrams predicting the flame behavior for a given set of flame and acoustic-flow properties. The influence of *Ma* on thermoacoustic instability is defined in the context of wrinkled thin premixed flames that are subject locally to weak curvature and/or flow-field strain [4]. *Ma* measures the sensitivity of local flame velocity and burning rate to curvature and stretch rate, characterizing the extent to effectively resist flame wrinkling. Previous works have shown that *Ma* has a strong influence on the acoustic instability of laminar premixed flames [3,6,8,18-20]. Clavin-Williams theory [5] provided an analytical expression of *Ma* whose value is sensitive to the internal structure of the flame represented by Zeldovich number (β), Lewis number (*Le*) and gas expansion (γ), which is extensively used in the formulation of stability diagrams [3, 9-11] using Searby and Rochwerger analysis [6]. Unfortunately, *Ma* from this expression is not accurate and shows limited validity for nearly equidiffusional flames whose (Le-1) is in the order of ($1/\beta$) [6]. Searby and Rochwerger used $Ma = 4.5 \pm 0.5$ in their work [6] but *Ma* from Clavin-Williams theory for lean propane-air flames would yield a value around 8.0. The incorrect prediction of *Ma* using the Clavin-Williams theory [5] was also previously pointed out to cause misprediction of critical acoustic velocity fluctuation amplitudes (U_a) on the onset of secondary instability [8,18] and complete instability of flat flames [3]. Because of these deviations, Aldredge [8,18] determined the value of *Ma* from U_a measurements using Laser Doppler velocimetry (LDV) at the onset of secondary instability of downward propagating flames in an annular burner, accounting for viscous damping [8]. However, *Ma* obtained from previous U_a measurements seems to have very large error bars and has not been experimentally validated against the wavenumbers at the onset of secondary instability. Furthermore, a dispersion of experimental and theoretical *Ma* also exists in the literature [19]. The motivation of the present work is to address this gap and to propose a simpler method to estimate *Ma* from experiments with downward propagating flames.

The purpose of this work is to introduce and validate a new approach to experimentally determine *Ma* by utilizing wavenumber measurements from the flame structure of methane-air flames at the onset of parametric instability. This approach may have some similarities to Aldredge [8,18]: however, we emphasize that the *Ma* estimation is based on wavenumber measurements whereas Aldredge [8,18] focused on U_a measurements. Furthermore, we employ the original formulation [6] and treat *Ma* as a free parameter, whereas Aldredge [8,18] employed the simplified explicit functions from Bychkov [7] to compute *Ma*. This method of determining *Ma* has not been previously explored. We then compare *Ma* for methane-air flames obtained by indirect and computational means in the literature.

2. Experimental method

A transparent acrylic combustion tube with 70.2 cm length (L) and 5 cm inner diameter is vertically fixed with a quartz glass bottom window. Initially, the tube is closed and is charged with premixed gases with around 20 times the combustion tube volume using Bronkhorst EL-Flow mass flow controllers at ambient pressure. The inlet and outlet valves are then closed, and premixed gases are contained for three minutes to become quiescent before spark ignition near the top end of the tube. The top lid opens simultaneously at the moment of ignition, rendering the boundary conditions amenable to that of a top-open and bottom-closed tube. Propagating flames are filmed using two synchronized high-speed cameras (FASTCAM Mini UX100 and AX200) at 2000 – 4000 FPS to capture the spatial and temporal evolution of the flame in frontal and lateral viewing angles depicted in Fig. 1. Prior trials are performed to set the focus of the bottom camera at the critical location (x) of parametric instability. Acoustic oscillations are measured using PCB Piezotronics 106B52 dynamic pressure sensor mounted at the closed end of the tube at 20 kHz sampling rate which is synchronized with video recording.

Methane-air premixed gases (calculated using CHEMKIN and GRI 3.0 mechanism [21]) were tested in the experiments. The test conditions were selected to fairly compare the experimental results at similar S_L in the lean and rich conditions where flat flames are observed before secondary instability. However, experiments in near- and stoichiometric conditions ($0.9 \leq \phi \leq 1.1$) show no flat flames in transition to parametric instability at L=70.2 cm. This complicates the interpretation of stability maps where D-L and parametric instability could coexist. To increase the band of acoustic velocity fluctuation amplitudes where planar flames are observed, the acoustic frequency must be increased [6]. Measurements for this range were realized by decreasing the tube length to 55.2 cm. The mixture properties and resonant frequencies are summarized in Table 1.

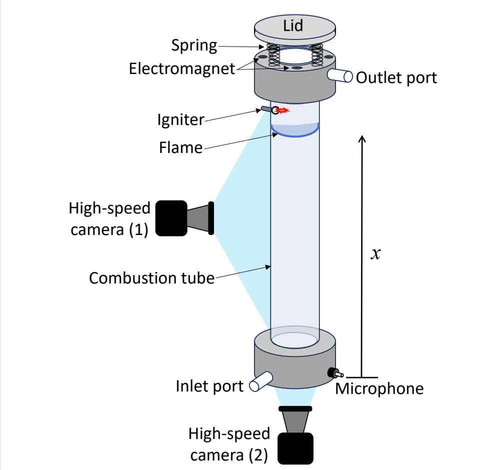

Fig. 1. Schematic diagram of the experimental setup.

Table 1. Properties and resonant frequencies of methane-air test mixtures.

Mix	S_L [cm/s]	ϕ [-]	T_b [K]	f [Hz]	L [cm]
1	25.01	0.769	1950	160	70.2
2	29.98	0.835	2050	175	70.2
3	34.22	0.9	2136	225	55.2
4	38.42	1.0	2230	226	55.2
5	38.79	1.1	2212	229	55.2
6	37.48	1.143	2181	175	70.2
7	35.01	1.189	2146	176	70.2
8	30.03	1.245	2100	175	70.2
9	25.04	1.280	2062	166	70.2

3. Theoretical method

The equation describing the time evolution of the flame front, whose amplitude is represented by F induced by acoustic forcing frequency ω_a, is based on the laminar flame model of Searby and Clavin [22], where Searby and Rochwerger [6] derived equations to calculate the limits and growth rate of instability of the perturbed flame depending on the wavenumber and amplitude of the induced acoustic wave.

$$A\frac{d^2F}{dt^2} + B\frac{dF}{dt} + [C_0 - C_1\cos(\omega_a t)]F = 0 \quad (1)$$

$$A = (2-\gamma) + \gamma\boldsymbol{k}\left(Ma - \frac{J}{\gamma}\right) \quad (2)$$

$$B = 2\boldsymbol{k} + 2\frac{\boldsymbol{k}^2}{1-\gamma}(Ma - J) \quad (3)$$

$$C_0 = \frac{\gamma\boldsymbol{k}}{Fr}\left[1 - \boldsymbol{k}\left(Ma - \frac{J}{\gamma}\right)\right] - \frac{\gamma}{1-\gamma} + \left\{\boldsymbol{k}^2 - \boldsymbol{k}^3\left[h_2 + \frac{\gamma+2}{\gamma}Ma - \frac{2J}{\gamma} + (2\,Pr - 1)H\right]\right\} \quad (4)$$

$$C_1 = \gamma\boldsymbol{k}\omega_a u_a\left[1 - \boldsymbol{k}\left(Ma - \frac{J}{\gamma}\right)\right] \quad (5)$$

Ma, *Pr*, *Fr* and γ refer to the Markstein number, Prandtl number, Froude number and gas expansion coefficient, respectively. $\boldsymbol{k}$ refers to the wavenumber (k) of the flame normalized by flame thickness (d). u_a is the imposed acoustic velocity amplitude (U_a) normalized by S_L. The details of integrals h_2, H and J in Eq. (2) – Eq. (5) can be found in [3,6-11]. Following Markstein's substitutions [4], Eq. (1) is transformed into a Mathieu equation representing a parametric response of a harmonic oscillator. The solutions of the Mathieu equation can also be found in [3,6,9-11]. For brevity, the calculation details are precluded in this context, and we adopt the method of determining the marginal stability limits in [3]. The boundary of marginal stability for parametric instability with contours of *Ma* for methane-air flame of Mixture 8 in Table 1 is shown in Fig. 2. The dotted line plots the locus of the onset of parametric instability when *Ma* is a free parameter. As seen in the figure, the critical wavenumber and acoustic velocity amplitude at the onset of parametric instability are clear functions of actual *Ma*. The boundaries for D-L instability are not shown here because the interest of the present work focuses on the cellular structure at the onset of parametric instability.

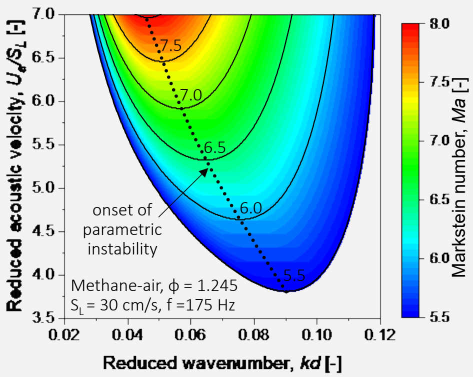

Fig. 2. Boundaries of marginal stability of parametric instability for methane-air flames at ϕ=1.245 for a range of *Ma* values. The onset of parametric instability changes at different values of *Ma* shown in dotted line.

4. Determination of Markstein number

This section describes the flame structures observed from experiments and discusses the process of *Ma* estimation based on wavenumbers at the onset of parametric instability. The process covers the (1) determination of the characteristic acoustic frequency at the onset of parametric instability to formulate stability diagrams similar to Fig. 2; (2) measurement of the wavelength (wavenumber) of the cellular flames; (3) estimation of *Ma* based on the wavenumber according to stability diagrams such as Fig. 2; and (4) validation of *Ma* against U_a based on pressure-time history.

4.1 Frequency determination

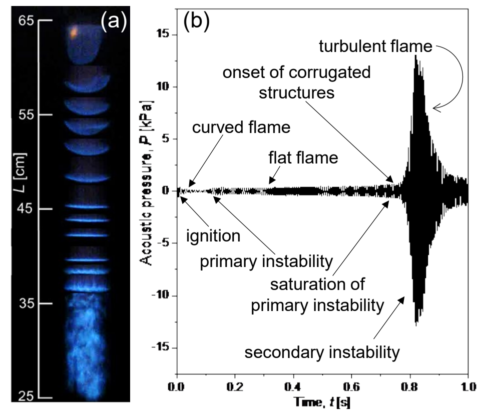

Fig. 3. Flame evolution (a) and pressure-time history (b) during flame propagation at ϕ=1.245.

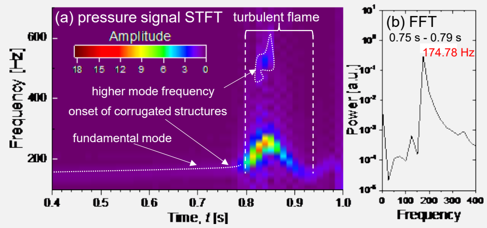

Fig. 4. (a) Variation of acoustic frequency during flame propagation. (b) FFT of the pressure signal 0.02s before and after the onset of parametric instability.

Figure 3 shows an example of (a) spatiotemporal evolution of the flame front and (b) corresponding pressure fluctuations at the closed end of the tube after ignition. The amplitude of acoustic oscillations gradually increases with time, and suddenly increases when parametric cellular structures appear at the location around x=38cm (t=0.77s). Short Time Fourier Transform (STFT) of the pressure signal in Fig. 4 (a) shows the change in frequency of oscillations with time. The dominant frequency of acoustic oscillations increases with time due to the increase in the overall temperature of the combustion tube. Once the flame is exposed to abruptly increased pressure oscillations ensuing from parametric instability, it turns to a turbulent regime. In this period, higher acoustic mode is observed, while only fundamental mode is observed at the moment of parametric instability. When parametric flame wrinkling appears at time t, the acoustic excitation is determined using FFT analysis at $t \pm 0.02$s as shown in Fig. 4 (b). The frequencies in each experiment do not vary appreciably and average values of repeated tests for each condition are shown in Table 1.

4.2 Wavenumber measurement

Flame structures during parametric instability of methane-air flames at different conditions are shown in Fig. 5 and Fig. 6 (also see the supplemental videos

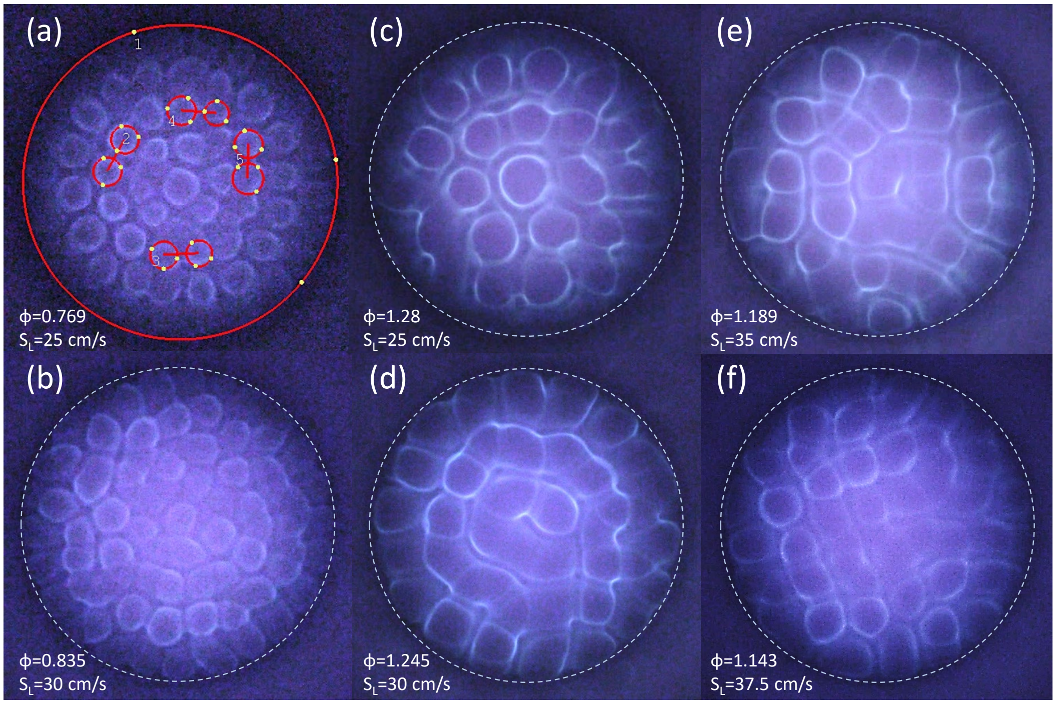

Fig. 5. Cellular flame structures at the onset of parametric instability of methane-air flames at *f*=160–176 Hz and tube length of 70.2 cm. The dashed lines indicate the cross-sectional area of the tube.

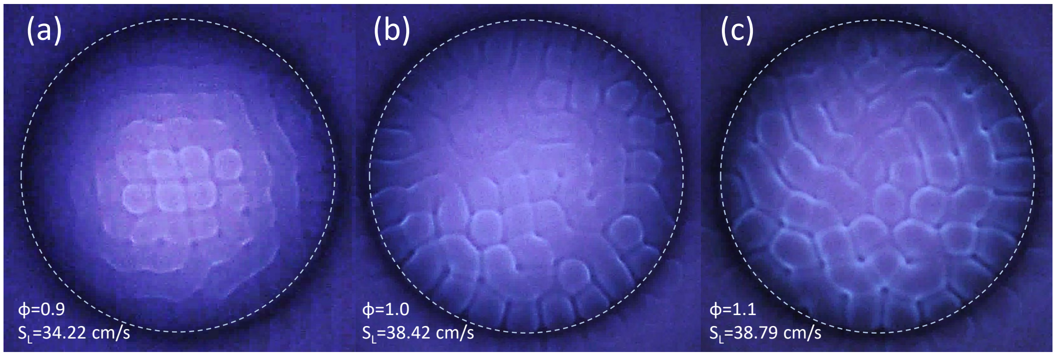

Fig. 6. Same with Fig. 5 but for near- and stoichiometric conditions at *f*=225–229 Hz and tube length of 55.2 cm.

showing how the cellular structures appear). At the right onset of parametric instability, the cells exhibit merged structures, and the edges of each cell are not well defined due to low amplitude sinusoidal flame wrinkling. After one or two pulsation cycles, the wavenumbers do not change but the amplitude of corrugation increases. The flame edges become more pronounced as seen in Fig. 5 and Fig. 6, with each cell being well-separated and a standing pattern is clearly observable. The influence of Le on cellular wavenumbers is evident when comparing flames at the same S_L. Lean methane-air flames ($Le \approx 0.96$) oscillate at larger wavenumbers compared to rich flames ($Le \approx 1.1$) as seen by comparing Fig. 5(a) with (c), or Fig. 5(b) with (d). Also, the wavenumber tends to increase with increasing S_L in the rich condition when comparing Fig. 5 (c) through (f). Similarly, the wavenumber decreases for near-stoichiometric conditions as the equivalence ratio increases in Fig. 6. Interestingly, parametric instability of methane-air flames tends to have symmetric structures at lower S_L, as can be observed at S_L=25 cm/s in Fig. 5 (a) and (c) where arrays of cells seem to circle around a larger cellular flame located at the center of the tube cross-section. This symmetry disappears when the S_L increases.

In measuring the wavenumber at the onset of parametric instability, the cells are averaged as circular during image processing. The wavelengths of sinusoidal flame wrinkling are determined by measuring the centroidal distance between adjacent cells as conceptually described in Fig. 5 (a). Wavelengths are measured only when there is a clear boundary between two adjacent cells. The tube cross-

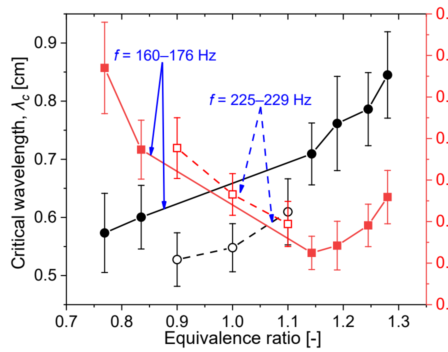

Fig. 7. Critical wavelengths and wavenumbers at the onset of parametric instability of laminar premixed methane-air flames for the range of equivalence ratios.

section can be traced by adjusting the brightness of the image and this serves as the scale for wavelength measurements. Wavelengths measured close to the wall versus those measured close to the center of the tube were found to not vary significantly as seen in Figs. 5 and 6. In each trial, at least 10 wavelength measurements can be obtained by analyzing one or two images during parametric instability. The wavelength (λ_c) and wavenumber (kd) of cellular flames measured from five experimental trials at each test condition are shown in Fig. 7, where $k=2\pi/\lambda_c$ and $d=D/S_L$ (D is the thermal diffusivity of the unburned mixture). The wavelengths tend to monotonically increase for the range of equivalence ratios, showing a larger wavenumber in lean conditions than those in rich conditions. Large wavenumbers of oscillating cells in lean flames should have larger flame surface area and induce larger heat release at the same S_L during parametric instability onset and lead to a higher growth rate of pressure oscillations observed in previous experiments [18]. It should be noted that the wavenumbers in the rich conditions do not show a consistent trend with the equivalence ratio contrary to the wavelength due to the difference in S_L and normalization with flame thickness.

4.3 Markstein number estimation and validation

As we have discussed in the previous section, the wavenumbers should correspond to the most unstable cell wavenumber when *Ma* is a free parameter in the calculation (see Fig. 2). To estimate *Ma* based on wavenumber measurements, the dependence of *Ma* on the onset wavenumber is plotted in *kd-Ma* plane by extracting the locus of the onset of parametric instability in the formulated stability maps as depicted by the dotted line in Fig. 2. The *kd-Ma* curves for each test conditions and range of forcing frequencies are shown in Fig. 8. For all test conditions, *Ma* decreases with increasing critical wavenumber. The right terminus of each curve indicates the minimum *Ma* where observation of flat flames is theoretically possible for respective mixtures and forcing frequencies in Table 1. The measured wavenumbers

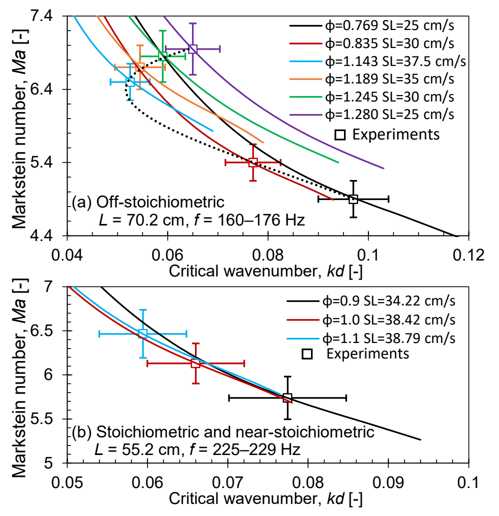

Fig. 8. Dependence of *Ma* on the critical wavenumber at the onset of parametric instability.

are fitted against these curves in Fig. 8 to find the most consistent *Ma* with experiments. Horizontal error bars represent the standard deviation of wavenumber measurements from experiments and vertical error bars show the potential variation of *Ma* corresponding to the experimental standard deviation.

Acoustic velocity fluctuation amplitudes are calculated based on measured pressure fluctuations at the bottom of the tube and tracking the location of the flame front. The particle displacement (ξ) of the unburned mixture at the combustion front can be calculated as $\xi = P_0 \sin(2\pi x/\lambda)/\rho_u c_u \omega_a$ [23]. P_0 refers to the amplitude of pressure fluctuation at the bottom end of the tube, and x is the distance of the flame front from the bottom end. λ is the wavelength of sound ($4L$) and ω_a refers to the circular acoustic frequency. ρ_u and c_u refer to the density and sound speed of the unburned gas, respectively. The acoustic velocity can be calculated as $u_a = d\xi/dt$.

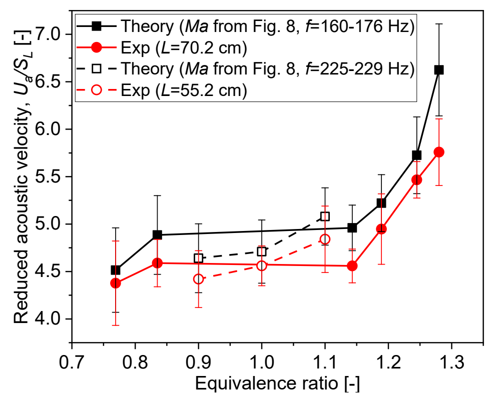

Fig. 9. Comparison of experimental and theoretical U_a at the onset of parametric instability. Theoretical acoustic velocities are derived from *Ma* obtained in Fig. 8.

The consequent U_a from *Ma* obtained in Fig. 8 is compared with the U_a estimated from the pressure data given by experiments as described above. Again, the *Ma*-U_a curve is extracted from stability maps as the dotted line in Fig. 2. The corresponding values of U_a to *Ma* are plotted to compare experimentally obtained values as shown in Fig. 9. In this figure, the acoustic velocity amplitude is normalized by S_L. The figure shows that the experimentally measured values are lower compared to theoretical values, but both values show a very consistent trend in the range of tested conditions.

5. Discussion

5.1 Applicability of the present method

The present approach is comparable to the method of Aldredge [8] because of the similarities of *Ma* measurement from thermoacoustically unstable flames. This method highly relies on the measurement of critical wavelengths and wavenumbers at the onset of parametric instability which necessitate the formation of flat flames before the transition. Hence, it is important that the formulation of stability maps, for a certain value of *Ma*, will lead to a band of U_a amplitudes where flat flames are observed, i.e. the D-L instability and parametric instability regions are well-separated. The difference in tube geometry is the main reason why flat flames cannot be observed in near-stoichiometric conditions at L= 70.2 cm in the present work compared to Aldredge [8,18] whose experiments employed a single tube length. Different flame regimes can be observed when the tube geometry is varied as discussed in our previous work [14]. As demonstrated in the present experiments, the acoustic frequency can be modulated by adjusting the tube length (sound wavelength). Increasing the frequency allows a wider band of U_a amplitudes for planar flames to occur [6]. This method can be used for a wide range of equivalence ratios and different types of gaseous fuels by carefully considering the S_L range and designing the geometrical parameters of the tube. However, this method in determining *Ma* may not be applicable for lean hydrogen-air flames whose *Le* is comparably very low than methane-air flames. Previous works suggest that due to the thermo-diffusive instabilities in lean hydrogen-air mixtures, the flame front cannot be planarized resulting in complete instability at all forcing frequencies and amplitudes [9,10]. Searby and Rochwerger [6] also mentioned that for rich propane-air mixtures whose *Ma* is known to be low [19,20,24,25], the planar flame is never stable for any acoustic intensity. For mixtures with slow chemistry like ammonia-air flames, parametric instability is unlikely to occur at very slow S_L (<10 cm/s) as observed in our previous experimental works [3,14]. Thus, this method is applicable for sufficiently fast flames with sufficiently large *Ma* where flat flames are observed before the transition to parametric instability.

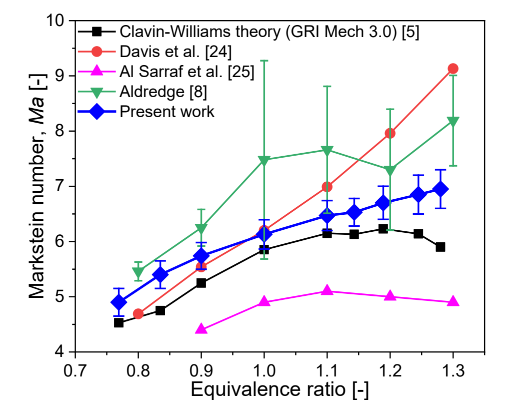

Fig. 10. *Ma* of methane-air flames versus equivalence ratio obtained from different methods.

5.2 Comparison of Markstein numbers obtained from various methods

Markstein numbers primarily emerge in S_L measurements from spherically expanding flames; however, they are not suitable for comparison with the *Ma* obtained in the present work. *Ma* in the formulation of Eq. (1) – Eq. (5) requires *Ma* relative to fresh gas and not to burnt gas, and the difference between the two may be quantitatively and qualitatively significant [24]. In this section, we exclusively compare *Ma* relative to fresh gas in the literature obtained from different methods as shown in Fig. 10.

Ma tends to increase with increasing equivalence ratio as a general trend, independent of researchers in Fig. 10. It is significant to note that there is good agreement between *Ma* obtained in the present work and those from Aldredge [8]. The lean case fits quite well, while the stoichiometric and rich cases seem to be within the error bars of those from [8]. However, the average results in the present work are smaller compared to [8]. A possible reason for this discrepancy could be attributed to the formulation of critical stability boundaries. Even if Aldredge [8] accounted the effects of viscous layers, this has a negligible effect on the onset of parametric instability. Their analysis also employed the simplified formulation of Bychkov [7] in computing *Ma*; however, the limiting conditions were not soundly satisfied so it was only used as an estimate [18]. In the present work, we employed the formulation originated from [6] and determined the critical point at the onset of parametric instability while treating *Ma* as a free parameter. Furthermore, the critical U_a reported by Aldredge [8] has very large error bars than the U_a obtained in this work. They used a 30 FPS camera in their recording while the present work operates at 2000–4000 FPS. The present frame rate is much higher than the time scale of the oscillating flame fronts. Deciding at what period to obtain U_a is crucial since the amplitude of pressure oscillations and acoustic velocity acting on the flame front drastically increase when cellular structures appear. By using two high-speed cameras capturing the longitudinal and lateral views of flame propagation, the present technique can accurately distinguish the parametric instability onset even at low-amplitude flame wrinkling. This crucial step is prone to errors when using a low FPS camera and capturing only one viewing angle since the onset of parametric instability shows mostly a planar flame in the lateral view when flame wrinkling amplitude is low. Wavenumber measurements also seem to be more efficient than U_a measurements in estimating *Ma* since at least 10 wavelengths can be measured in one experiment while only one U_a can be obtained from each experiment. Even so, consistent with Aldredge [8], the *Ma* obtained in the present work are underpredicted by Clavin-Williams theory [5]. Consistencies are also found in comparison with computational *Ma* obtained by Davis et al. [24] from methane-air counterflow flames where *Ma* increases monotonically in the range of equivalence ratio as shown in Fig. 10. Interestingly, *Ma* in the present work converges with Davis et al. [24] in the stoichiometric condition, while the lean and rich cases have larger and smaller values, respectively. It should be noted that the equation leading to the Mathieu function and the critical wavenumbers at the onset of parametric instability is based on activation energy asymptotic analysis which is governed by one-step Arrhenius law and large Zeldovich number [6,22], whereas *Ma* obtained by Davis et. al [24] are based on finite rate and multi-step chemical kinetics which depend on detailed chemistry and transport models. Also, the quantitative significance of *Ma* may vary with different flame configurations; however, we compared *Ma* with counterflow flames because it was subsequently discussed in the previous analysis of Aldredge [8], which also shows reasonable agreement with the present results. On the other hand, Al Sarraf et al. [25] indirectly estimated *Ma* by fitting the theoretical and experimental growth rate of D-L instability of methane-air flames propagating in a quasi-2D Hele-Shaw burner using a modified dispersion relation. Heat loss and viscous damping are the major drawbacks of their *Ma* estimation which reduces the growth rate of instability [25]. Their determination of the growth rate of D-L instability is very complicated where the wavenumber of the hydrodynamically perturbed flame cannot be held fixed and there is a local birth and merging of cellular flames during flame propagation. The growth rate of D-L instability attenuates in the presence of acoustic field [6-11] but this effect in narrow channels was not discussed in [25]. The temperature-dependent diffusivities were also simplified using the relation $\rho D \propto T^{0.5}$ [25] while this work calculated the integrals in Eq. (2) – (5) in detail from CHEMKIN libraries. Surprisingly, despite the losses, *Ma* obtained from the previous study [25] are smaller compared to the present work. Other flame configurations and methods for determining *Ma* relative to fresh gases are consolidated and described in [19,25]; however, these values are significantly lower than the *Ma* obtained in the present work.

6. Conclusion

This work developed a new method and demonstrated a simple, efficient, and retroactive approach to estimate the Markstein number relative to fresh gases by investigating the flame structure of thermoacoustically unstable premixed flames. Parametric instability of downward propagating laminar premixed methane-air flames in open-closed tubes was studied by synchronized high-speed imaging and pressure fluctuation measurements. A clear transition of planar flames to cellular flames during parametric instability was presented for the first time. The Markstein number of laminar premixed methane-air flames was indirectly determined from wavenumber measurements at the onset of parametric instability by employing the laminar flame model under acoustic excitation and treating the Markstein number as a variable parameter. Acoustic velocity fluctuation amplitudes derived from pressure oscillation measurements ascertained the validity of Markstein numbers obtained from wavenumbers measurements. Agreement was found with Markstein numbers obtained from numerical simulations in counterflow methane-air flames. The Markstein numbers obtained in the present study are between the values obtained from previous LDV measurements and Clavin-Williams theory.

Declaration of competing interest

The authors declare that they have no known competing financial interests or personal relationships that could have appeared to influence the work reported in this paper.

Acknowledgments

This study was supported by JSPS KAKENHI Grant Number JP22H01408.

References

[1] J.W.S.B. Rayleigh, The explanation of certain acoustical phenomena, Nature 18 (1878) 319–321.
[2] G. Searby, Acoustic instability in premixed flames, Combust. Sci. Technol. 81 (1992) 221–231.
[3] A.K. Dubey, Y. Koyama, S.H. Yoon, N. Hashimoto, O. Fujita, Range of “complete” instability of flat flames propagating downward in the acoustic field in combustion tube: Lewis number effect, Combust. Flame 216 (2020) 326–337.
[4] G. H. Markstein, Non-steady flame propagation, Pergamon Press, New York, 1964.
[5] P. Clavin, Dynamic behavior of premixed flame fronts in laminar and turbulent flows, Prog. Energy Combust. Sci. 11 (1985) 1–59.

[6] G. Searby, D. Rochwerger, A parametric acoustic instability in premixed flames, J. Fluid Mech. 231 (1991) 529–543.
[7] V. Bychkov, Analytical scalings for flame interaction with sound waves, Phys. Fluids. 11 (1999) 3168–3173.
[8] R.C. Aldredge, Methane-air Markstein numbers from measurements of thermoacoustic instability, Combust. Sci. Technol. 177 (2005) 1023–1047.
[9] J. Yáñez, M. Kuznetsov, R. Redlinger, The acoustic–parametric instability for hydrogen-air mixtures, Combust. Flame 160 (2013) 2009–2016.
[10] J. Yáñez, M. Kuznetsov, J. Grune, Flame instability of lean hydrogen-air mixtures in a smooth open-ended vertical channel, Combust. Flame 162 (2015) 2830–2839.
[11] A.K. Dubey, T. Tezuka, Y. Morii, H. Nakamura, K. Maruta, Acoustic parametric instability in thermo-diffusively unstable CH4/O2/Xe mixtures, Combust. Flame 258 (2023) 113056.
[12] S.H. Yoon, T.J. Noh, O. Fujita, Onset mechanism of primary acoustic instability in downward-propagating flames, Combust. Flame 170 (2016) 1–11.
[13] S.H. Yoon, T.J. Noh, O. Fujita, Effects of Lewis number on generation of primary acoustic instability in downward-propagating flames, Proc. Combust. Inst. 36 (2017) 1603–1611.
[14] A.K. Dubey, Y. Koyama, N. Hashimoto, O. Fujita, Effect of geometrical parameters on thermo-acoustic instability of downward propagating flames in tubes, Proc. Combust. Inst. 37 (2019) 1869–1877.
[15] A.K. Dubey, Y. Koyama, N. Hashimoto, O. Fujita, Exploring a critical diameter for thermo-acoustic instability of downward propagating flames in tubes, Proc. combust. Inst. 38 (2021) 1945-1954.
[16] A.K. Dubey, Y. Koyama, N. Hashimoto, O. Fujita, Experimental and theoretical study of secondary acoustic instability of downward propagating flames: higher modes and growth rates, Combust. Flame 205 (2019) 316–326.
[17] V. Vaezi, R.C. Aldredge, Laminar-flame instabilities in a Taylor-Couette combustor, Combust. Flame 121 (2000) 356–366.
[18] R.C. Aldredge, N.J. Killingsworth, Experimental evaluation of Markstein number influence on thermoacoustic instability, Combust. Flame 137 (2004) 178–197.
[19] F. Veiga-López, D. Martínez-Ruiz, M. Kuznetsov, M. Sánchez-Sanz, Thermoacoustic analysis of lean premixed hydrogen flames in narrow vertical channels, Fuel 278 (2020) 118212.
[20] F. Veiga-López, D. Martínez-Ruiz, E. Fernández-Tarrazo, M. Sánchez-Sanz, Experimental analysis of oscillatory premixed flames in a Hele-Shaw cell propagating towards a closed end, Combust. Flame 201 (2019) 1–11.
[21] G.P. Smith, D. Golden, M. Frenklach, N.W. Moriarty, B. Eiteneer, M. Goldenberg, C.T. Bowman, R. K. Hanson, S. Song, W. C. Gardiner, Jr., V.V. Lissianski, and Z. Qin, GRI Mech 3.0, http://combustion.berkeley.edu/gri-mech/
[22] G. Searby, P. Clavin, Weakly turbulent, wrinkled flames in premixed gases, Combust. Sci. Technol. 46 (1986) 167–193.
[23] W.E. Kaskan, An investigation of vibrating flames, Symp. (Int.) Combust. 4 (1953) 575–591.
[24] S. G. Davis, J. Quinard, G. Searby, Markstein numbers in counterflow, methane-and propane-air flames: a computational study, Combust. Flame 130 (2002) 123–136.
[25] E. Al Sarraf, C. Almarcha, J. Quinard, B. Radisson, B. Denet, P. Garcia-Ybarra, Darrieus-Landau instability and Markstein numbers of premixed flames in a Hele-Shaw cell. Proc. Combust. Inst. 37 (2019)1783–1789.